Geophysical Journal International

Geophys. J. Int. (2016) **206,** 1515–1525
Advance Access publication 2016 June 14
GJI Geodynamics and tectonics

doi: 10.1093/gji/ggw225

Present-day dynamic and residual topography in Central Anatolia

Ebru Şengül Uluocak,[1] Russell Pysklywec[2] and Oğuz H. Göğüş[3]

[1]*Department of Geophysics, Canakkale Onsekiz Mart University,* 17020 *Canakkale, Turkey. E-mail: ebrusengul@gmail.com*
[2]*Department of Earth Sciences, University of Toronto, M5S 3B1 Toronto, ON, Canada*
[3]*Eurasia Institute of Earth Sciences, Istanbul Technical University,* 34469 *Ayazaga, Istanbul, Turkey*

Accepted 2016 June 10. Received 2016 June 9; in original form 2015 August 31

SUMMARY

The Central Anatolian orogenic plateau is represented by young volcanism, rapid plateau uplift and distinctive (past and active) tectonic deformation. In this study, we consider observational data in terms of regional present-day geodynamics in the region. The residual topography of Central Anatolia was derived to define the regional isostatic conditions according to Airy isostasy and infer the potential role of 'dynamic topography'. 2-D thermomechanical forward models for coupled mantle-lithosphere flow/deformation were conducted along an N–S directional profile through the region (e.g. northern/Pontides, interior and southern/Taurides). These models were based on seismic tomography data that provide estimates about the present-day mantle thermal structure beneath the Anatolian plate. We compare the modelling results with calculated residual topography and independent data sets of geological deformation, gravity and high surface heat flow/widespread geothermal activity. Model results suggest that there is ∼1 km of mantle flow induced dynamic topography associated with the sublithospheric flow driven by the seismically inferred mantle structure. The uprising mantle may have also driven the asthenospheric source of volcanism in the north (e.g. Galatia volcanic province) and the Cappadocia volcanic province in the south while elevating the surface in the last 10 Myr. Our dynamic topography calculations emphasize the role of vertical forcing under other orogenic plateaux underlain by relatively thin crust and low-density asthenospheric mantle.

Key words: Mantle processes; Dynamics of lithosphere and mantle; Dynamics: convection currents, and mantle plumes; Dynamics: gravity and tectonics; Asia.

1 INTRODUCTION

Central Anatolia is characterized by plateau-type topography of ∼1 km mean elevation and it borders the East Anatolian compressional province in the east and Western Anatolia extended terranes in the west (Fig. 1a). Geodetic data show westward motion of Central Anatolia of ∼21 mm yr^{-1} with respect to the fixed Eurasian Plate (e.g. Reilinger *et al*. 2006; Özeren & Holt 2010). In the north, this motion is accommodated by the North Anatolian Fault (NAF), a right lateral strike slip fault between Anatolia and the Eurasian Plate. According to geological and geomorphological interpretations, the Central Anatolian Plateau has attained its present-day elevation during the last 10 Myr, associated with more than 1 km of surface uplift (Cosentino *et al*. 2011; Yildirim *et al*. 2011; Schildgen *et al*. 2012). Specifically, the southern section of Central Anatolia (Taurides)—represented by 2 km of present-day elevation—is dominated by the deposition of widespread marine sediments suggesting that the area has been rising since the Early Miocene. Furthermore, nearly 1 km of surface uplift has been documented by river incision studies in the northern Pontides (Yildirim *et al*. 2013) and the interior portion of the Central Anatolian Plateau; e.g. Cappadocia Volcanic Province (Aydar *et al*. 2013; Çiner *et al*. 2015; Fig. 1b). While the origin and cause of the uplift over the entire plateau has remained elusive, there is convincing evidence that suggests the plateau uplift and regional tectonic evolution may have been driven by vertical forcing (e.g. mantle driven) rather than plate shortening. For instance, Cosentino *et al*. (2011) argues that the sedimentary rocks of the southern margin (namely, the Mut and Ermenek Basins) of the plateau do not contain features of tectonic deformation (i.e. folding and faulting) in the last 8 Myr. According to Özsayin *et al*. (2013) an interior basin of Central Anatolia, the Tuz Gölü Basin, has been controlled by normal faulting in the last ∼6 Myr. The magnitude of presumed approximately N–S oriented extension over the plateau is uncertain; such extension has also been reported in the north, near the Galatia Volcanic Province (GVP; Yürür *et al*. 2002; Fig. 1b).

Estimates of regional gravity anomalies provide insights into the regional geodynamics and these can be used to infer the component of isostatic versus dynamic compensation for a variety of areas around the globe such as Africa (Hartley *et al*. 1996), Australian continent (Simons *et al*. 2000), Western Anatolia (Komut *et al*. 2012) and the Western US (Becker *et al*. 2014). In this respect, Özelçi (1973) points out the inverse relationship between gravity data and observed topography in Anatolia and adjacent regions (e.g. deep marine basins around the Mediterranean) in light of the

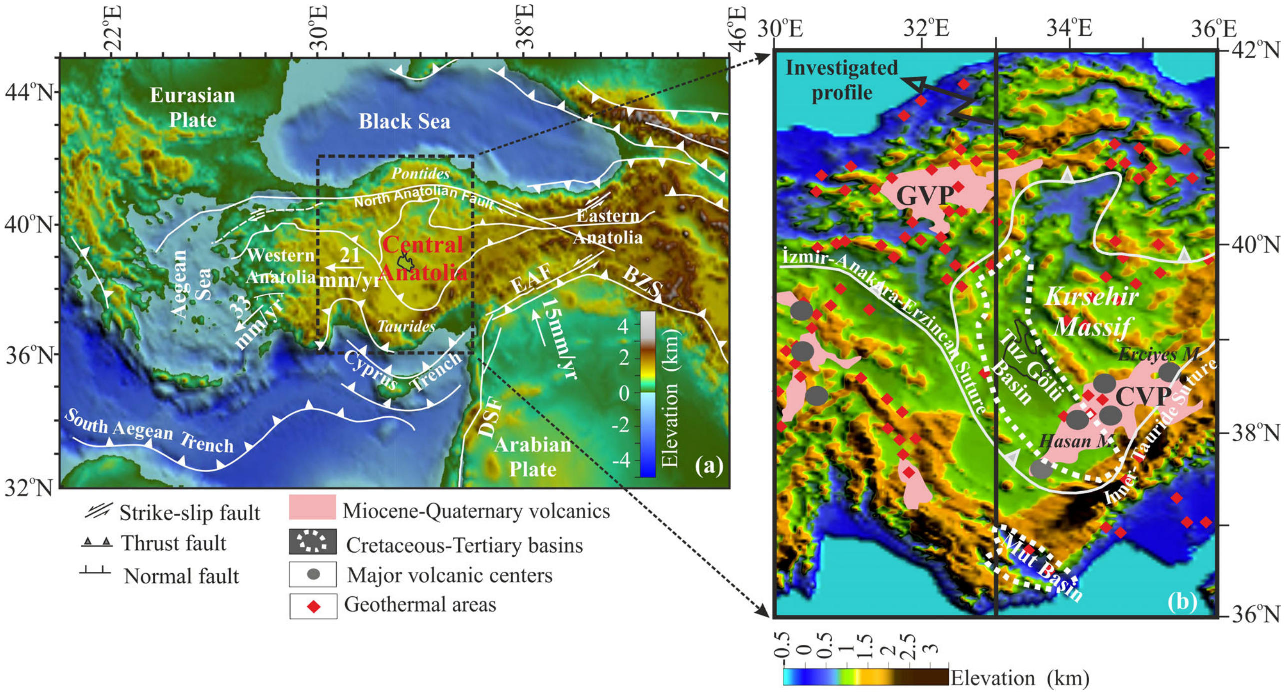

Figure 1. Topography map of the region (Amante & Eakins 2009; ETOPO1). (a) Major boundaries and tectonic units of the study area (after Şimşek 2001; Jolivet *et al*. 2009; Biryol *et al*. 2011). (b) Neotectonics, volcanic features and geothermal fields of Central Anatolia (simplified from Şimşek 2001; Huvaz 2009; MTA 2014, the high-resolution background topographic relief is obtained from GLOBE 2014). DSF; Dead Sea Fault, BZS; Bitlis-Zagros Suture, CVP: Cappadocia Volcanic Province, GVP: Galatia Volcanic Province, M: Mountain.

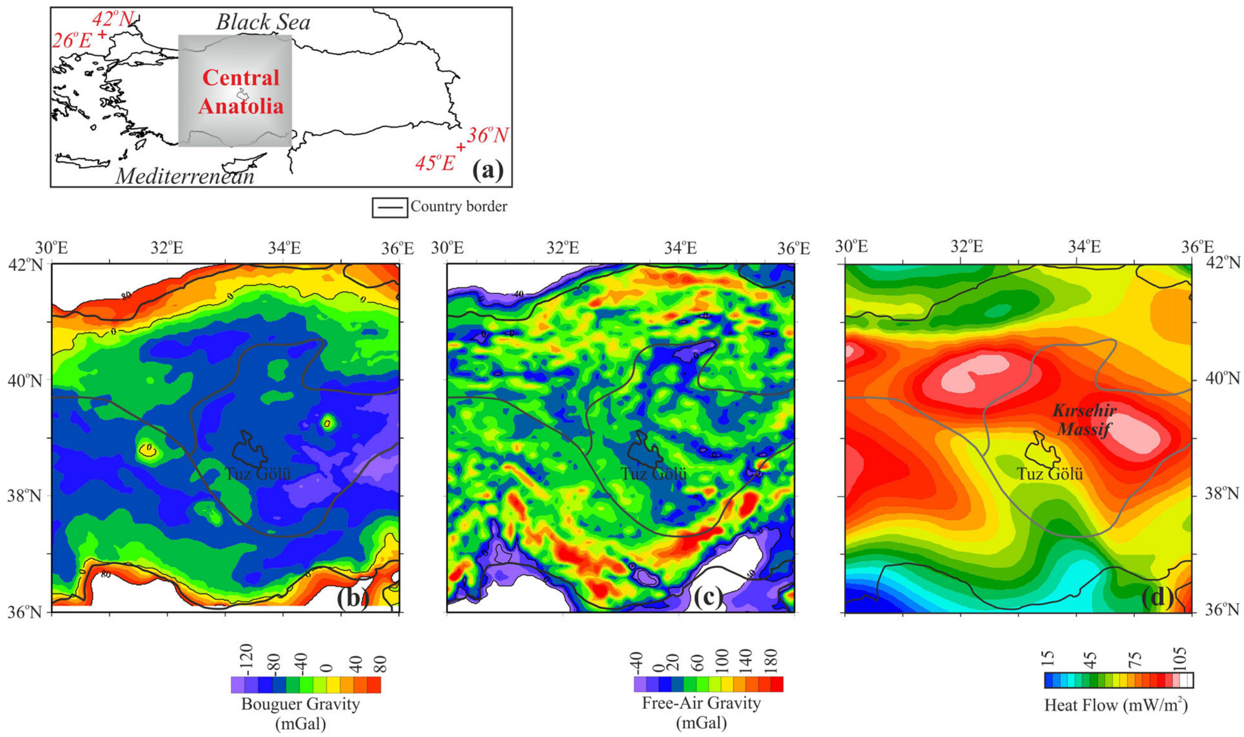

Figure 2. (a) Location map of Central Anatolia, (b) Bouguer gravity map (compiled from Ateş *et al*. 1999), (c) free air gravity map (compiled from EGM2012; Bonvalot *et al*. 2012) and (d) surface heat flow map of Central Anatolia (Tezcan 1995; Aydin *et al*. 2005).

documented geological features. More specifically, the author suggests that the Bouguer gravity anomalies are approximately 80–100 mgal higher than the expected range because of asthenospheric mantle upwelling beneath the Anatolian crust. Fig. 2(b) shows high Bouguer anomalies for Central Anatolia (compiled from Ateş *et al*. 1999). Free air anomalies can be a good indicator of the isostatic conditions in a region. For instance, Kumar *et al*. (2009) analysed the Bouguer and free air gravity signature along a profile (250 km long) in South India and indicated a broad positive correlation between observed topography and free air as well as negative correlation

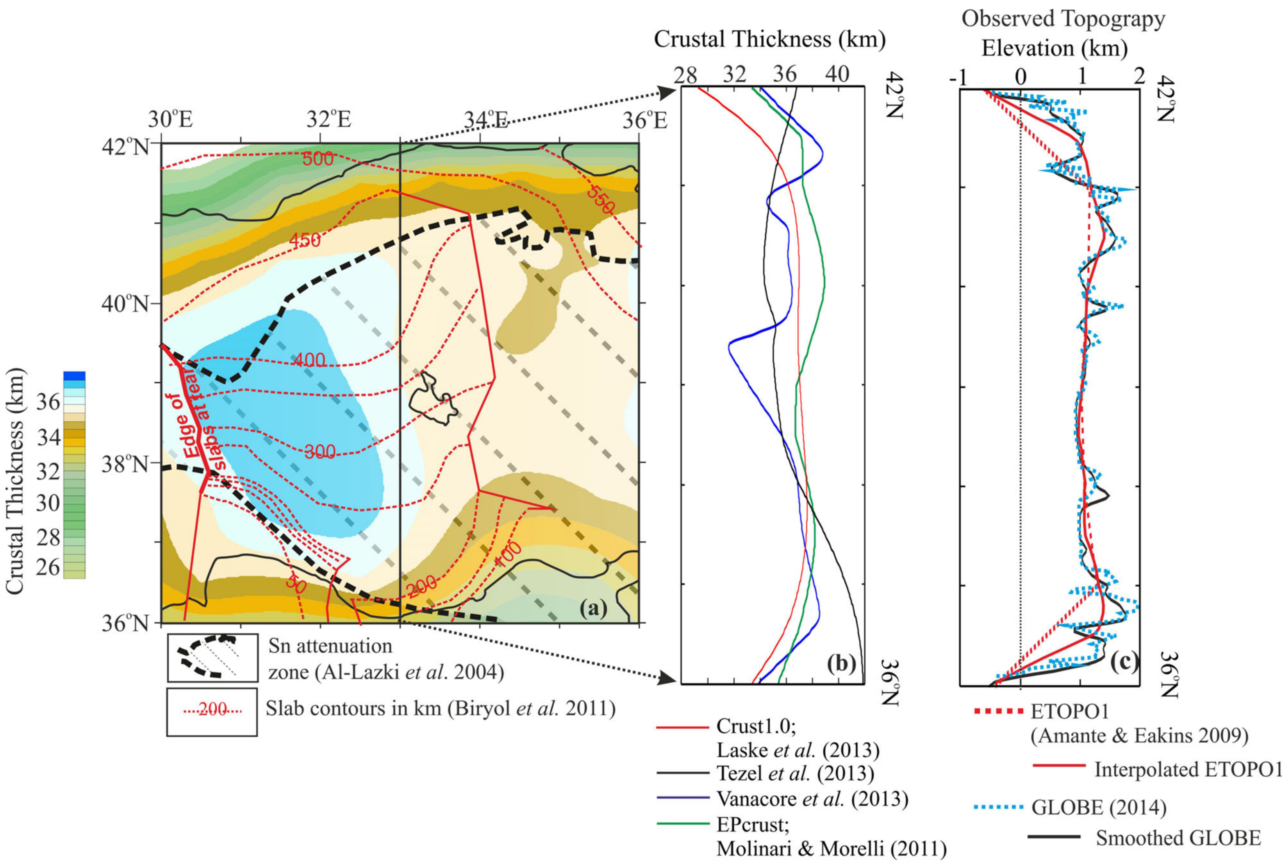

Figure 3. (a) The map of the crustal thickness obtained from the Crust1.0 database (Laske *et al*. 2013). The black hatched area indicates a zone of high Sn attenuation (Al-Lazki *et al*. 2004). The contours show the surface depth of the slabs beneath Central Anatolia based on Biryol *et al*. (2011). (See Fig. 2a for geographic location). (b) The cross-section of different crustal thicknesses along the investigated profile based on various data sets (Crust1.0; Tezel *et al*. 2013; Vanacore *et al*. 2013; EPcrust: Molinari & Morelli 2011). (c) Cross-sections of observer topographies based on ETOPO1 and GLOBE and re-gridded form of these data sets.

with Bouguer anomalies. In addition to the lithological and major structural elements in the region, they estimate that the low free-air value (~-5 mGal) state overcompensation resulted from a mass deficit at subcrustal depth in the region (Kumar *et al*. 2009). In another case, a high free air anomaly correlated with the topography shows under compensation in Western Anatolia (Komut *et al*. 2012). Arslan *et al*. (2010) characterizes Central Anatolia as having high free air gravity values. Similarly, a free air gravity map compiled from the Earth Gravitational Model (EGM2012; Bonvalot *et al*. 2012) shows high free air anomalies inconsistent with the high topography especially in the northern and southern parts of the area (Fig. 2c).

Central Anatolia is also characterised by widespread geothermal activity in relation to high surface heat flow, volcanism and shallow Curie-point depth (CPD) observations. Tezcan & Turgay (1991) proposed high surface heat flow estimates ($\sim$70–100 mW m^{-2}) based on geothermal gradients by using exploration wells in the region. Similarly, Central Anatolia shows high heat flow values ($\sim$100 mW m^{-2}) based on the surface heat flow rate map for Europe (Chamorro *et al*. 2014). Tezcan (1995) also suggests that Central Anatolia is associated with high heat flow anomalies, although such anomalies diminish in the northern and southern part of the region due to the relatively high sediment thickness there. Fig. 2(d) shows the surface heat flow distribution for Central Anatolia. In addition, rather shallow Curie-point contours at $\sim$12–14 km depth based on aeromagnetic anomalies in the region (e.g. Ateş *et al*. 2005; Aydin *et al*. 2005) correlate well to the Central Anatolian Volcanics (such as the Cappadocia, Erciyes and Hasan Mountain Volcanic complexes) and Yozgat Massif. Furthermore, the volcanism is presumed to originate from asthenospheric sources under Cappadocia Volcanic Province (CVP; Kürkçüoğlu *et al*. 2004) and the GVP in relation to regional extension (Tankut *et al*. 1998).

In agreement with the asthenosphere-driven high surface heat flow anomalies, various sets of seismic tomography data indicate the presence of low seismic velocities beneath Central Anatolia which may be caused by upwelling of asthenospheric mantle (e.g. Gök *et al*. 2003; Piromallo & Morelli 2003; Al-Lazki *et al*. 2004). Biryol *et al*. (2011) indicate high seismic velocities related to the subducted African lithosphere along the Cyprian and the Aegean trenches beneath Anatolia based on nonlinear inversion of teleseismic traveltime data. They imply that the gaps between the subducted Cyprus and Aegean slabs are occupied by slow/hot upwelling asthenosphere which forms a hot crust and related surface structures such as the Quaternary Central Anatolia Volcanics. The authors also draw these fast anomalies as slab contours by tracing upper surfaces of the Aegean and Cyprian slabs which are consistent with the regional P tomography of Piromallo & Morelli (2003) in terms of northward deepening cold structures (a simplified form of their slab contours for Central Anatolia is shown in Fig. 3a). Recent full-waveform inversion tomography results show that the low velocities at 75 km depth are localized directly beneath the Central Anatolian Volcanics related to their thermal origin (Fichtner *et al.* 2013a,b). Fichtner *et al.* (2013a) interpret these anomalies as shallow upwelling asthenosphere in the region. Higher attenuation rates of Pn and Sn waves have also been suggested—in the uppermost mantle beneath the Central Anatolian crust—[i.e. attenuation for Sn waves (Fig. 3a) and relatively slower propagation of Pn waves $<7.9\ \mathrm{km\ s^{-1}}$; Hearn & Ni 1994; Al-Lazki *et al.* 2004]. Seismological interpretations by Vinnik *et al.* (2014) suggest that the lithosphere is only 60 km thick beneath the interior part of the Central Anatolian plateau according to the inversion of *P*- and *S*-wave velocities and dispersion curves of Rayleigh waves. More recently, Kind *et al.* (2015) shows that the lithosphere–asthenosphere boundary is in the range of 85 km depth beneath Central Anatolia based on S-receiver function analyses conducted in Turkey and its surrounding areas.

Pn wave anisotropy orientations show high variations within Anatolia (e.g. Al-Lazki *et al.* 2004). Kömeç-Mutlu & Karabulut (2011) suggest that very small Pn anisotropy anomalies are observed between 33°E and 37°E where low Pn velocities are obtained. They show generally N–S fast axis orientation in the western part of Central Anatolia (west of 33°E). Al-Lazki *et al.* (2004) indicates that Pn anisotropy fast axes can be mainly defined as N–S in the central part of the Anatolian plateau, and there is no clear relationship between observed Pn anisotropy orientations and Eurasia fixed GPS vector directions. Paul *et al.* (2014) defines a considerable amount of shear-wave azimuthal anisotropy in the Aegean–Anatolian region, and shows a relatively uniform widespread NE–SW fast orientation by comparing SKS splitting data with Pn anisotropy, upper-mantle wave velocity, and global mantle flow models (Paul *et al.* 2014 and references therein). Besides, unlike the previous studies (e.g. Biryol *et al.* 2010) they speculate that fast retreat of the south Aegean trench is much more effective than weaker rollback of the Cyprean slab on the NE–SW split orientations from the Aegean to Anatolia (Paul *et al.* 2014). This approach is consistent with mantle flow models explaining the regional scale flow driven by suction from the south Aegean slab combined with the large scale mantle flow forming the Mediterranean tectonics (e.g. Forte *et al.* 2009; Faccenna & Becker 2010; Faccenna *et al.* 2014; Paul *et al.* 2014; Yolsal-Çevikbilen 2014; Göğüş 2015). These major mantle flow directions roughly fit with geodetic data indicating Anatolia's motion with respect to Eurasia (e.g. Faccenna & Becker 2010). However, the relatively slower westward motion of the Isparta Angle (the movement is almost two times slower in the east than the western part of the angle relative to Eurasia; Barka & Reilinger 1997), in which not only conspicuous Pn anisotropy is observed but deviation from uniform splitting direction, is defined as an obstacle to the westward motion of Central Anatolia by the flow of asthenospheric mantle accommodated by slab tears (e.g. Biryol *et al.* 2011; Kömeç-Mutlu & Karabulut 2011). According to Paul *et al.* (2014), the uniform NE–SW direction is not supported by the absolute plate motion (APM) velocities in the region; the APM velocities correlated to weak surface strain are E–W in most of Central Anatolia (Paul *et al.* 2014). In contrast to the northern and central part of the region, the local Pn anisotropy pattern is obtained in the Taurides which are the main tectonic unit in the south, located parallel to the Cyprus arc—in accordance with the perturbation of SKS maximum horizontal stretching directions at 150–170 km in depth (Al-Lazki *et al.* 2004; Paul *et al.* 2014). In the north, while average SKS splitting orientations are uniform across the NAF zone (e.g. Biryol *et al.* 2010), the western and eastern parts of the NAF are roughly separated around the central Pontides based on Pn anisotropy and Pn station delay times (e.g. Al-Lazki *et al.* 2004; Kömeç-Mutlu & Karabulut 2011). An in-depth analysis of these controversial seismic anisotropy structures in the region is beyond the scope of this paper. However, in general while the uniform NE–SW direction addresses large scale instantaneous density–driven mantle flow in the upper mantle, the low Pn velocities correlated with relatively larger delay times and higher Pn anisotropy distribution might be due to ongoing/increased mantle deformation in the hot anisotropic asthenosphere beneath Central Anatolia (e.g. Sandvol *et al.* 2003).

The regional map of crustal thickness obtained from Crust1.0 (Laske *et al.* 2013) based on averages of a global database of crustal thickness data from both receiver function and active source seismic studies is shown in Fig. 3(a). Crustal thickness estimates from other studies in the region are also shown as N–S cross-sectional profile at 33°E in Fig. 3(b). Fig. 3(c) illustrates cross-sections of the observed topographies from ETOPO1 (Amante & Eakins 2009) and the global land one-km base elevation project GLOBE (GLOBE Task Team *et al.* 1999). Crust and topographic data were resampled to the same grid resolution (9 km east × 9 km north directions) with a linear interpolation algorithm (e.g. Shaw & Pysklywec 2007). The gridding process can make data more comparable but also interpolate or smooth the data (i.e. ETOPO1 at 1 × 1 degrees are interpolated, whereas high-resolution GLOBE is slightly smoothed as shown in Fig. 3c). In that case, average values of these crustal thicknesses along the profile are obtained as a mean value ± standard deviation; 36.07 ± 1.7 km in Vanacore *et al.* (2013), 36.97 ± 2.5 km in Tezel *et al.* (2013), 36.13 ± 1.7 km for Crust 1.0 (Laske *et al.* 2013) and 37.21 ± 1 km in EPcrust data (Molinari & Morelli 2011). Generally, there is a good correlation between these studies for the interpreted Moho depth variations (nearly a flat Moho at ∼36 km) within the plateau interior (Figs 3a and b) although some variations on the northern and southern shoulders of the plateau have been postulated in crustal studies (e.g. Tezel *et al.* 2013; Vanacore *et al.* 2013). Overall, seismological studies claim that the mantle lithosphere is significantly thin beneath Central Anatolia as the plateau is underlain by hot sublithospheric mantle with 36 km thick crust in the central region.

The crust and the lithosphere beneath Central Anatolia are hot, relatively thin and isostatically uncompensated considering the present day elevation. In this work, we investigate the role of rising active upper mantle in potentially creating anomalous topography which may be responsible for the >1 km of uplift and dynamic support in Central Anatolia. We first consider the nature of the inferred regional uplift by calculating topography residuals (non-isostatic component of topography) with the available regional crustal thickness data. Subsequently, these data are reconciled against the geodynamic model predictions of the dynamic topography using the translation of *P*-wave seismic tomography model to temperature domain as the inferred lithosphere/mantle structure beneath Central Anatolia. Our model predictions based on 2-D temperature variations along an N–S profile (33°E) are slightly oblique to the NE–SW orientations of the SKS fast axes and involves some simplification of the complex tectonics (e.g. Shaw & Pysklywec 2007). However, we focus on the vertical component of 3-D upper-mantle flow in the form of mantle flow-induced dynamic topography and its correlation with the surface deformations in a young and active orogenic plateau like Central Anatolia.

2 UPLIFT OF CENTRAL ANATOLIA

2.1 Residual topography

Residual topography is considered to be the difference between the observed topography and the corrected topography based on the approximation for isostatic compensation (usually Airy) of the crust. For instance, residuals with a positive deflection show that the surface topography is higher than what would be expected assuming isostatic adjustment and surface topography from the average densities within the lithosphere (e.g. Heiskanen & Meinesz 1958). Accordingly, residual topography calculations are made by removing the isostatic contribution from observed topography using the principle of Airy isostasy while assuming crustal blocks are in hydrostatic equilibrium in the mantle. In such a case, complete compensation considers that topographic loading is supported by buoyancy forces moving on the surface of equilibrium in consequence of variations in crustal thickness in the region. Here, we made our isostatic calculations based on the following formula given by Gvirtzman & Nur (2001);

$$h_{\mathrm{res}} = h_{\mathrm{o}} - h_{\mathrm{calc}} - H_0 \tag{1a}$$

$$h_{\mathrm{calc}} = [(\rho_{\mathrm{m}} - \rho_{\mathrm{c}})/\rho_{\mathrm{m}}]\, H_{\mathrm{c}}, \tag{1b}$$

where h_{res} is residual topography, h_{o} is observed elevation, h_{calc} is the calculated isostatic topography obtained from chosen crustal thickness (H_{c}) and average densities (ρ_{m} and ρ_{c} are mantle and crustal densities, respectively). H_0 is a constant that shifts amplitude up or down statically, thus the amplitudes of the residual topography field can be relative. For example, Lachenbruch & Morgan (1990) suggest that this value would be 2.4 km for mid-ocean ridges by considering a standard column of oceanic lithosphere (e.g. 2.6 km in Faccenna *et al*. 2014). In such a case, it is possible to avoid relatively local isostatic variations such as subducting slabs by defining the lowest residual topography expected from a thick lithosphere (e.g. Gvirtzman & Nur 2001). This approach defines an absolute residual topography (ART) which may useful for global studies and flow calculations. However, in this study we focused on regional variations of residual topography instead of ART to compare such results locally and also directly with dynamic topography obtained from regional thermomechanical models (calculated in a 'local' closed box but with higher resolution of lithospheric features) as described the following section. Therefore in this study, H_0 was calculated as an average value of the calculated isostatic topography (mean value of $\mathrm{h}_{\mathrm{calc}}$) to reduce residuals to the reference level. We also compiled global databases as the input data—Crust1.0 (Laske *et al*. 2013) for the crustal thickness and ETOPO1 (Amante & Eakins 2009) for the topography—to investigate the regional effects of the residual topography in Central Anatolia. Densities were defined as $\rho_{\mathrm{m}} = 3300$ kg m^{-3} for mantle and $\rho_{\mathrm{c}} = 2840$ kg m^{-3} for crust. With these data and eqs (1a) and (1b), the region yields a positive residual elevation (the map of residual topography; RT1 in Fig. 4a) by taking a reference level as 4.49 km).

RT2 and RT3 were calculated based on different databases to show the influence of data resolution on the residual anomaly. While RT2 was calculated using high-resolution GLOBE (GLOBE Task Team *et al.* 1999) data together with the same crustal thickness as RT1 (i.e. Crust1.0, shown in Fig. 3a), RT3 was predicted from ETOPO1 and EPcrust databases in Central Anatolia (reference levels used were 4.49 km for RT2; 4.7 km for RT3). All input data were used with the same grid size as mentioned in the Introduction for the residual topography calculations. The mean values ± standard deviation for RT1, RT2 and RT3 are: 0.916 ± 0.26, 0.984 ± 0.33 and 1.00 ± 0.31 km, respectively (Fig. 4b). There is a good correlation between residual topographies in terms of main signal trends and average values of amplitudes along the profile, however the lateral resolution of input data (i.e. high-resolution topography) affects the amplitude of residuals at shorter wavelength (∼200 km

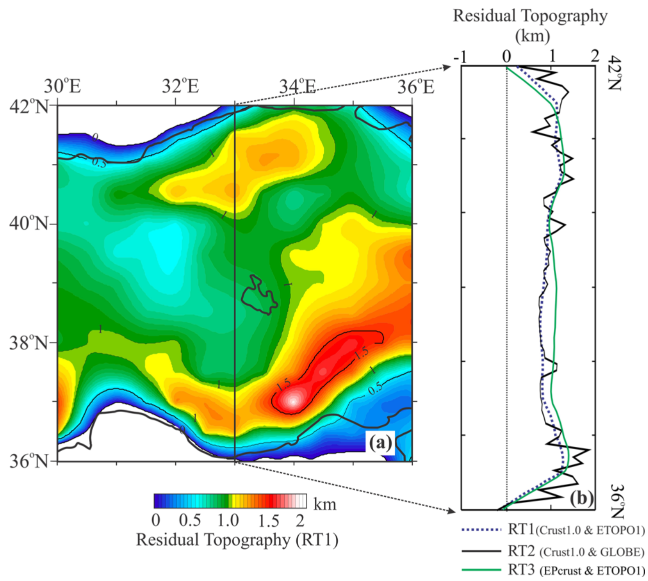

Figure 4. (a) Residual topography map (RT1). (b) Cross-sections of residual topography calculations RT1, RT2 and RT3 (see the text for full explanation).

or less as stated in Flament *et al*. 2013) as shown in Fig. 4(b). As well as input data resolution, density variations can also modify the results for residual topography calculations. The various densities obtained from global databases and the literature (such as Crust1.0) for the crust and mantle were tested on residual topography calculations along the profile. The test results indicate that uniform density variations do not have an effect on modifying residual topography.

The residual topography calculations suggest that the interior/central part of Central Anatolia is associated with nearly 1 km of anomalous plateau-like topography and that observed topography is undercompensated. Positive topography residuals increase on the plateau shoulders with more than 1 km in the north and exceeding 1.5 km in the south. The enhanced uplift at the southern margin may be due to local tectonic effects, as suggested by paleoelevation studies (e.g. Schildgen *et al*. 2012; Aydar *et al*. 2013).

We note that although surface erosion and deposition have been shown to have a significant impact on surface and deep lithospheric tectonics (e.g. Pysklywec 2006; Gray & Pysklywec 2012), these effects can be ignored as well as the non-uniform density variations and local heterogeneities in the input data to investigate the regional characteristic of the residual topography in the region (e.g. Shaw & Pysklywec 2007). Instead, we consider signal patterns and average amplitudes of residual topography for comparison.

2.2 Present-day geodynamic modelling in Central Anatolia

Topography that is induced by mantle flow is one of the main products of geodynamic models and is called 'dynamic' (Pekeris 1935; Flament *et al*. 2013 and references therein). In this study, we conducted a series of numerical experiments to investigate if the residual portion (anomalous) topography of Central Anatolia can be explained by mantle flow induced dynamic topography. The basis for the mantle convective driving forces is derived from the *P*-wave seismic tomography data of Piromallo & Morelli (2003) that gives a 'snapshot' of the mantle structure perpendicular to the orientation of the Cyprus arc along 33°E (Figs 5a and b). This N–S cross-section is taken along the seismic tomography profile

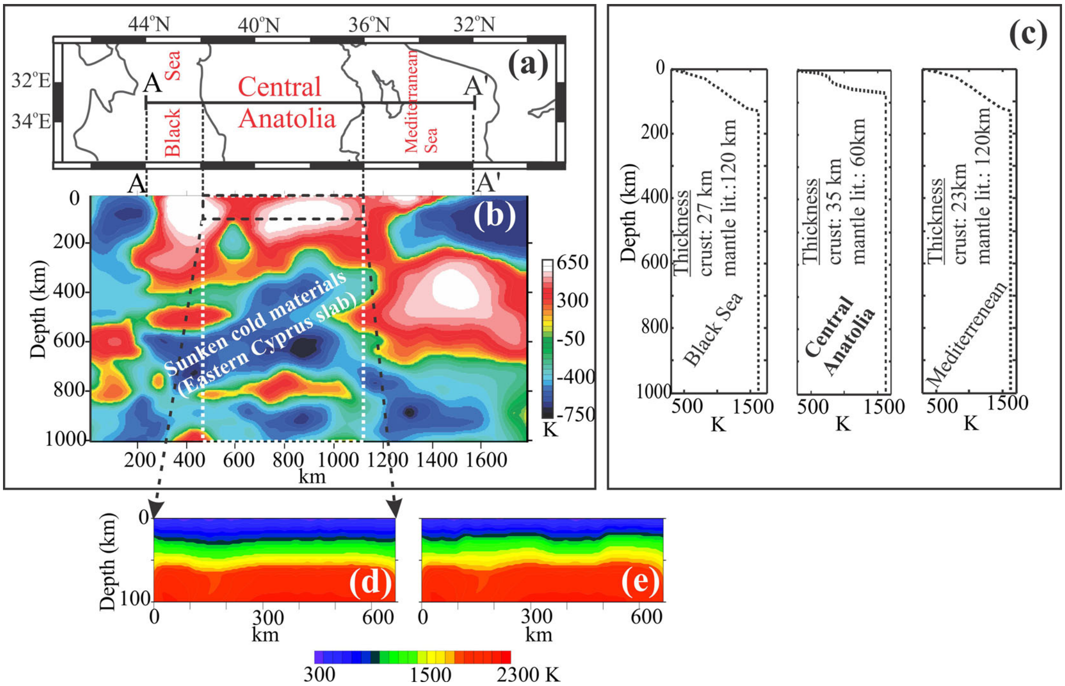

Figure 5. (a) Location of the investigated profile. (b) 2-D temperature cross-section from *P*-wave tomography (white dotted rectangle shows temperature variations beneath Central Anatolia). (c) The schematic diagram of the normal geotherms. Temperature anomalies in lithospheric scale for (d) the mantle-based and (e) the crust-based models beneath Central Anatolia.

(e.g. A–A′) and it is in close approximation with the residual topography estimates discussed in the previous subsection. Our modelling procedure begins by digitizing the *P*-wave seismic traveltime tomography data obtained by inversion of the *P*-wave delay time (i.e. for up to 1000 km depth, from Piromallo & Morelli 2003; Faccenna *et al*. 2006) into roughly 9 km horizontal × 10 km vertical grid sampling for the thermal input in the numerical calculations. The *P*-wave velocity variations from the tomography inversion have been converted into density anomalies. This conversion was based on the depth dependent density scaling variations from the function of $\delta\ln\rho/\delta\ln v$ versus depth that was made in approximation for the global symmetric spherical energy loss distribution (see Chopelas & Boehler 1989; Karato 1993) for selected *P*-wave velocities. Then, the density anomalies, $\rho(T)$, were translated into thermal anomalies by using the equation of thermal expansion:

$$\rho(T) = \rho_0 (1 - \alpha \Delta T), \tag{2}$$

where ρ_0 is reference density (kg m^{-3}), α is the coefficient of thermal expansion (K^{-1}) and ΔT (K) is the change in temperature relative to a background temperature field (e.g. Shaw & Pysklywec 2007). The background temperature values (normal geothermal field) can be calculated based on conductive equilibrium in the thermomechanical models. The temperature is set to vary linearly from the base of the lithosphere to the asthenospheric mantle, 793 to 1623 K in the initial model (Fig. 5c). Furthermore, to verify our initial thermal condition and presume closer approximation for Central Anatolia's underlying temperature field, we defined thermal conductivity coefficient ($\kappa = 2.503$ W m^{-1} K^{-1}) and average surface temperatures based on Chamorro *et al*. (2014) along the profile, and also assigned a free surface to CPD (∼14 km) as 285 K to 772 K in the initial model parameters based on observational data for Central Anatolia (Fig. 5c).

In the geodynamic model, the temperatures derived from the *P*-wave seismic tomography data are not at high resolution on a crustal scale (Fig. 5b). Thus, we defined only normal geotherms instead of superimposed temperature values in the crust and refer to them as mantle-based models (i.e. Models 1, 2 and 3) since the crust is more stable in terms of lateral temperature variations in mantle-based models (Fig. 5d). We also considered in a separate model lateral temperature heterogeneities in Central Anatolian crust to determine the influence of thermal data resolution in this region. Model 1 (reference model; Table 1) was modified roughly comparing the model results with the surface heat flow anomalies (Fig. 2d) along the profile (the crust-based reference model; Model 4, Fig. 5e). Owing to the modelling procedure based on a forward solution, we conducted a series of tests by changing temperature values empirically in the crust to obtain more refined crustal features in Central Anatolia compared to just using the tomography data.

In light of this crustal and mantle thermal configuration, we calculated flow/deformation within the section using a 2-D Arbitrary Lagrangian Eulerian (ALE) finite element method with the SOPALE numerical modelling code for solving large scale geodynamic problems (e.g. Fullsack 1995; Pysklywec *et al*. 2002; Göğüş & Pysklywec 2008a,b). A free surface at the top of the model is used; therefore surface topography was free to develop in response to the underlying flow dynamics. In regards to material composition and configuration, we defined three different layers in the model design (Fig. 6). From surface to depth, these are wet quartzite crust, wet olivine lithospheric mantle beneath crust and wet olivine asthenospheric mantle beneath the lithosphere. Numerical calculations were run by Eulerian grid size of 201 horizontal × 101 vertical nodes. Based on the geophysical constraints, we considered average values of the crustal and lithospheric thickness along the N–S profile—36 and 24 km, respectively—for Central Anatolia as stated in the introduction. The sidewalls and bottom of the solution box were free-slip and a heat flux of zero was assigned to the sidewalls. Although the top surface of the model was defined as the free surface, erosion

Table 1. Mechanical parameters of the reference model; Model 1 (e.g. Gleason & Tullis 1995; Hirth & Kohlstedt 1996).

Mechanical parameters	Crust	Mantle lithosphere	Asthenospheric mantle
Reference density (ρ_0; kg m^{-3})	2840	3300	3300
Reference temperature (T_0; K)	293	293	293
Interval of internal friction angle (Q; degree)	[15, 15]	[15, 12]	[15, 12]
Range of the second invariant of the strain rate ($\dot{\varepsilon}$)	[0.5, 1.5]	[0.5, 1.5]	[0.5, 1.5]
Viscosity parameter (B; Pa^{-n} s^{-1})	1.1×10^{-28}	4.89×10^{-15}	4.89×10^{-15}
Power exponent (n)	4	3.5	3.5
Activation energy (Q; kJ mol^{-1})	223	515	515
Specific heat capacity (c_p; J kg^{-1} K^{-1})	750	750	750
Thermal conductivity (κ; W mK^{-1})	2.503	2.25	2.25
Thermal expansivity (α; K^{-1})	2.0×10^{-5}	2.0×10^{-5}	2.0×10^{-5}

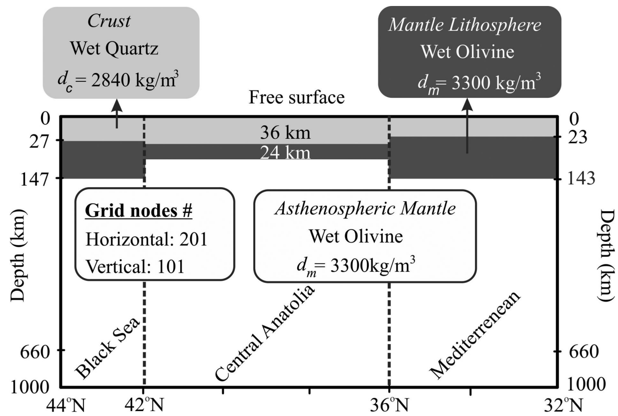

Figure 6. 2-D setup parameters for the thermomechanical models (unscaled).

and/or sedimentation were not considered in our study. The governing equation and formulation of viscous-plastic rheology used in the model are given as (Fullsack 1995);

$$\nabla . v = 0 \tag{3}$$

$$\nabla . \sigma_{ij} + \rho g = 0 \tag{4}$$

$$\frac{\mathrm{D}T}{\mathrm{D}t} = \kappa \nabla^2 T + \frac{H}{\rho c_\mathrm{p}}. \tag{5}$$

In the above equations, v is velocity (m s^{-1}), g is gravitational acceleration (10 m s^{-2}), T is temperature (K), κ is thermal diffusivity (m^2 s^{-1}), t is time (s), c_p is specific heat capacity (J kg K^{-1}) and H is the rate of internal heat production per unit mass (W m^{-3}) (Table 1). Eqs (2)–(5) define conservation of mass, momentum and internal energy, and hence thermal buoyancy drives motion in the interior and surface of the solution space. The deformation of the materials at high temperature is governed by a viscous-plastic rheology. For this, the deviatoric stress tensor σ' calculated at each node as $\sigma' = \min\{\sigma_v; \sigma_y\}$ is the minimum of a plastic yield stress (σ_y) or viscous stress (σ_v) where

$$\sigma_y = p \sin\phi + C_0 \tag{6}$$

$$\sigma_v = 2\eta\dot{\varepsilon}. \tag{7}$$

Here, ϕ is angle of internal friction (degrees), C_0 is cohesion (Pa) and p is total pressure. A nominal value internal friction angle $\phi_{1,2}$ = 15° for the crust determines the plastic yield stress (Pysklywec & Beaumont 2004). In addition, $\phi_1 = 15°$ to $\phi_2 = 12°$ linearly decreases over a strain range of 0.5 to 1.5 for the mantle in the reference model configuration. A cohesion of 1 MPa is used for the crust and mantle. For viscous stress, the effective viscosity (η) is a function of the second invariant of the deviatoric strain rate tensor ($\dot{\varepsilon}$) and the temperature:

$$\eta(\dot{\varepsilon}, T) = B^{-1/n} \varepsilon^{(1/n-1)} e^{Q/nRT}, \tag{8}$$

where B is viscosity parameter (Pa^{-n} s^{-1}), n is non-Newtonian viscosity exponent, Q is activation energy (J mol^{-1}) and R is universal gas constant (8.31 J mol^{-1} K^{-1}). The transition zone at 660 km depth is defined with a discrete increase in viscosity (as 100-fold) at this depth in the model. In our model predictions, we focus on different rheological properties for the viscous creep strength coefficients (Table 1). Accordingly, while Model 2 defines a 'strong model' where the upper- and lower-mantle viscosities have been increased by an order of magnitude, Model 3 indicates a 'weak model' where the viscosity of the mantle has been decreased by a factor of 10 compared to the reference model (Model 1).

Fig. 7(b) shows the mantle flow with the computed velocities for the reference model (Model 1). As can be inferred from the figure the temperature-dependent viscosity variation in this model means that the crust and lower mantle have a high viscosity, while the underlying mantle (above 660 km depth) has a lower viscosity. The velocity vectors in the mantle show rising mantle under the crust associated with the circulation of material (mainly) in the upper mantle. The associated dynamic topography predicted by Model 1 is characterized as a broad plateau-type elevation (~1 km) along the profile between 42°N and 36°N (Fig. 7b).

The mantle flow pattern and the viscosity variation for the stronger mantle model (Model 2) are shown in Fig. 7(c). Compared to the previous model, the upwelling mantle flow and the associated pattern of the symmetry is prone to decrease towards the northern section (42°N) of the profile. This is a result of a more constrained flow in this part of the mantle where subducted slab material has accumulated. The surface topography of this model reflects this asymmetry in flow with less uplift towards the north since the decreased flow velocity there yields lessened normal stresses at the surface that drives surface elevation. We note that over 1 km of elevation persists over most of the Central Anatolian portion of the profile (Fig. 7c).

As an alternative experiment Fig. 7(d) shows Model 3. In this model, as expected, the magnitude of the circulation velocity is higher and the flow develops more vigorously through the entire upper mantle. The associated surface topography is still plateau-type uplift with higher peaks in the northern and southern margins (Fig. 7d). The magnitude of predicted topography (~900 m) is less in this experiment compared with the previous two models. We carried out strong and weak alternatives to the crust-based reference model (Model 4) based on different viscous creep strength coefficients in

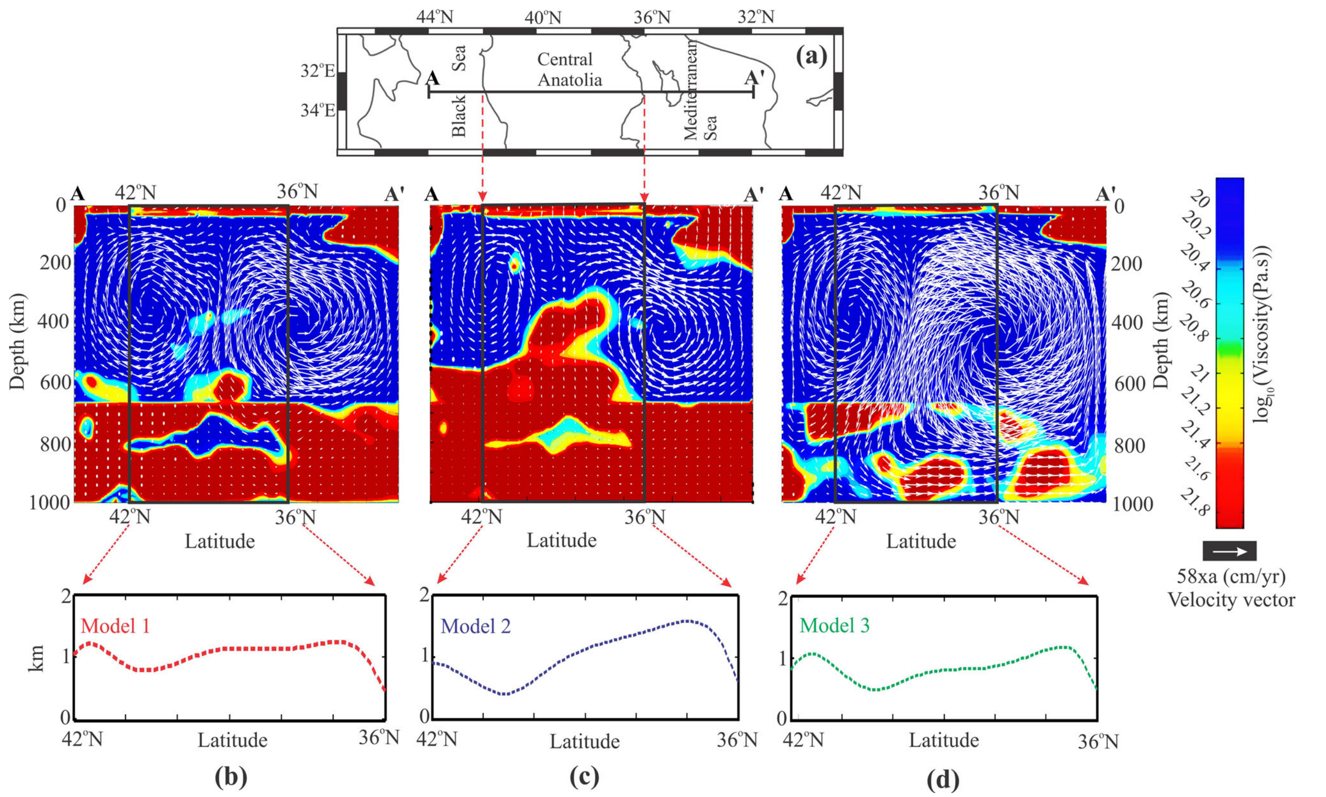

Figure 7. (a) Location of the investigated profile. Cross-sections of the convection flow velocity vectors with the viscosity variations (on the top) and the geodynamic topography (on the bottom) for three different mantle-based models (black frames shown under Central Anatolia). (b) Model 1: reference model, (c) Model 2: strong model, (d) Model 3: weak model (grid samplings are 30 km for each directions, and the vector scaling parameter is $a = 2$ in the velocity maps).

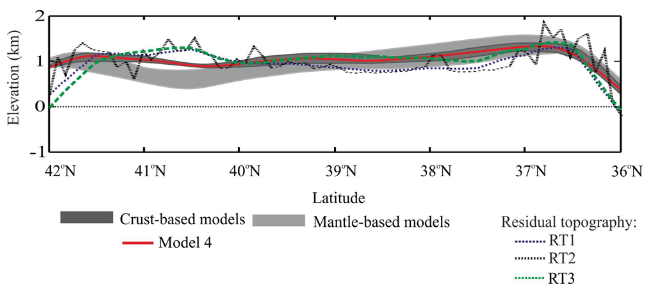

Figure 8. Residual topography and dynamic topography ranges of mantle- and crust-based models according to the different viscous rheology. The average dynamic topography is 0.95 ± 0.27 km for the mantle-based models and 1.00 ± 0.14 km for the crust-based models.

the crust as the topographic responses of these models are simply shown as a range in Fig. 8.

The surface topography variations predicted by the different experiments are compared with the calculated residual topography in Fig. 8 and in general, the patterns and amplitudes of the anomalies are consistent. Mantle-based models offered the main plateau-type topographic profile with the average amplitude of 0.95 ± 0.27 km based on the upper-mantle flow beneath the region. The crust-based models sensitive to lateral temperature heterogeneities in the crust produced 1.00 ± 0.14 km elevation as shown in Fig. 5(e).

The average values of the surface heat flow calculated from the thermomechanical models based on the temperature anomaly with constant thermal conductivity value along the profile are 78.0 ± 5.5 and 83.5 ± 5.5 mW m^{-2} for mantle-based and crust-based models, respectively.

3 RESULTS AND DISCUSSION

Residual topography calculations clearly indicate that elevated topography is not supported by crustal thickness based on the principle of Airy isostasy in Central Anatolia. This result emphasizes the presence of an under compensated plateau in concordance with the high free air and Bouguer gravity anomalies over the region (Fig. 2).

In this work, thermomechanical models of crust-mantle deformation were run using available *P*-wave tomography data to estimate the current mantle structure along the N–S profile which is oblique to general NE–SW shear wave splitting orientation as interpreted from seismic anisotropy studies in the region (e.g. Paul *et al*. 2014). The predicted dynamic topography based on vertical components of density–driven flow in the upper mantle is mainly induced by 2-D temperature variations beneath Central Anatolia. This mantle structure drives a non-isostatic component of topography that we compare with the observed topography residuals. Further we tested the response of the models to different viscous creep strength coefficients and temperatures. The dynamic topography ranges predicted from these experiments are shown in Fig. 8. As described in the previous section, mantle-based models characterize the main dynamic uplift range based on the upper-mantle flow beneath the region. The average dynamic support is obtained as ∼1 km from the suite of thermomechanical models (Fig. 8). A comparison of the residual topography with the dynamic topography indicates that, although some secondary discrepancies emerge at shorter wavelengths (≤200 km), there is regional consistency in terms of anomaly pattern and amplitude of the observed versus predicted surface topography along the investigated profile (Fig. 8).

The models produce especially large upper-mantle flow velocity vectors in the southern part of the profile (Fig. 7b). The cold materials related to deep Cyprus slab fragments in our temperature section track to the main trend of the southward rising slab surfaces as shown in Fig. 3(a). However, discontinuity of this structure allows northward asthenosphere upwelling in the south (Fig. 5b). When compared with the central and northern regions, this flow causes slightly increased dynamic topography in the south where relatively high residual and observed topography are obtained (Figs 3c and 8). This result might indicate the possible effect of predominant upper-mantle-flow-induced deformations in the southern margin of Central Anatolia as supported by the local Pn anisotropy anomalies around the Taurides as described in the Introduction.

Dynamic elevations decrease in the north because of a cold local structure that causes a downwelling anomaly in the upper mantle (in Fig. 5b, a high seismic velocity located in between N40°–N41° and 100–250 km depth). This cold anomaly does not appear at high resolution and possibly is not connected to the surface (e.g. Faccenna *et al*. 2006). Our model results are inadequate to resolve this uncertainty because it is outside of our solution space, yet it can't be ruled out that this is roughly located under complex structural boundaries; for instance, in Biryol *et al*. (2011) this region is defined as the south edge of the Western Pontide Fragment based on *P*-wave traveltime tomography data (fig. 9 DC′ section in Biryol *et al*. 2011). This zone also appears to be a transition zone between eastern and western parts of the NAF according to Pn anisotropy and Pn station delay times. Further, one can speculate that this local anomaly might be associated with the deep effects of the NAF in the upper mantle. Fichtner *et al*. (2013b) suggest that crustal features of the NAF zone are governed by weak Tethyan sutures—that formed 60–15 Ma ago—at greater depth (∼100 km) based on a multiscale full waveform inversion approach. However, there is no indication of a deep lithospheric extent of the NAF based on high-resolution surface wave tomography images (Salaün *et al*. 2012), SKS splitting measurements (Paul *et al*. 2014) and S-receiver functions analyses (Kind *et al*. 2015). In our interpretation, high-resolution crustal thickness, or/and *P*-wave seismic data could resolve this mismatch between residual and dynamic patterns shown in Fig. 8. Additionally, as suggested by Boschi *et al*. (2010), upper-mantle-scale high-resolution shear wave velocity data might be used as input data for modelling studies to explain local structures in this region. Regional variations of the data sets (such as crustal thickness and seismic data) are considered here and positive residual and dynamic topography resulting from geodynamic features in Central Anatolia are obtained.

4 CONCLUSIONS

The dynamic topography predictions demonstrate an uplift representing an instantaneous response of the surface to underlying mantle flow for Central Anatolia. The high surface heat flow anomaly calculated from the numerical experiments indicates hot Central Anatolian crust consistent with the observed widespread geothermal activity, young volcanism and metamorphic massifs in the region. These results are partly compatible with previous broader geodynamic studies in the region. For instance, Boschi *et al*. (2010) define the Central Anatolian Plateau as having high dynamic elevation—with different amplitudes and lateral anomaly patterns (e.g. $\sim > 1$ km for Schmid model in Boschi *et al*. 2010) based on 3-D numerical models using upper-mantle-scale 3-D seismic data in the Mediterranean Basin. Bartol & Govers (2014) focused on lithospheric properties beneath the Aegean–Anatolian–Near East region to explain geodynamic evolution resulting in present-day surface features in the overriding plate. They calculated a 3-D thermonumerical model including 20 Myr periods by assuming the volcanism and uplift in the Central and Eastern Anatolian Plateau occurred simultaneously, and ignoring the local lateral heterogeneities such as the slab fragment gaps between these two regions. According to the testable part of their lithospheric scenario, Central and Eastern Anatolia formed as a single plateau since the middle Miocene without any crustal thickening in the Central Anatolian Plateau. Considering previous studies in the region, geodynamic models and related evaluations are consistent in their context; however, there are some limitations based on the initial assumptions, resolution and sensitivity areas of chosen primary data sets. For instance, present-day geodynamic models based on forward solutions produce data-dependent results as shown in our results above. Nevertheless, by taking into account a direct comparison of observables and experiments based on several independent data sets, our results provide robust new information about the regional dynamic component of the topography obtained from geodynamic models and residual topography calculations in the region.

ACKNOWLEDGEMENTS

Authors acknowledge support from TUBITAK Visiting Scientist fellowship programme. RP acknowledges funding from an NSERC Discovery Grant. Numerical calculations were done using a modified version of the SOPALE (2000) software. The SOPALE modelling code was originally developed by Phillip Fullsack at Dalhousie University with Chris Beaumont and his Geodynamics group. We thank the anonymous reviewers and Laurent Husson for their useful comments and contributions to the manuscript.

REFERENCES

Al-Lazki, A.I., Sandvol, E., Seber, D., Barazangi, M., Turkelli, N. & Mohamad, R., 2004. Pn tomographic imaging of mantle lid velocity and anisotropy at the junction of the Arabian, Eurasian, and African plates, *Geophys. J. Int.*, **158,** 1024–1040.

Amante, C. & Eakins, B.W., 2009. *ETOPO1 1 Arc-Minute Global Relief Model: Procedures, Data Sources and Analysis,* NOAA Technical Memorandum NESDIS NGDC-24, 19 pp.

Arslan, S., Akin, U. & Alaca, A., 2010. Investigation of crustal structure of Turkey by means of gravity data, *Bull. Miner. Res. Explor.,* **140,** 57–73.

Ateş, A., Kearey, P. & Tufan, S., 1999. New gravity and magnetic anomaly maps of Turkey, *Geophys. J. Int.,* **136,** 499–502.

Ateş, A., Bilim, F. & Büyüksaraç, A., 2005. Curie point depth investigation of Central Anatolia, Turkey, *Pure appl. Geophys.,* **162,** 357–371.

Aydar, E., Cubukcu, H.E., Sen, E. & Akin, L., 2013. Central Anatolian Plateau, Turkey: incision and paleoaltimetry recorded from volcanic rocks, *Turk. J. Earth Sci.,* **22,** 739–746.

Aydin, İ., Karat, H.İ. & Koçak, A., 2005. Curie-point depth map of Turkey, *Geophys. J. Int.,* **162,** 633–640.

Barka, A. & Reilinger, R., 1997. Active tectonics of the Mediterranean region: deduced from GPS, Neotectonics and seismicity data, *Ann. Geofis.,* **40,** 587–610.

Bartol, J. & Govers, R., 2014. A single cause for uplift of the Central and Eastern Anatolian plateau?, *Tectonophysics,* **637,** 116–136.

Becker, T.W., Faccenna, C., Humphreys, E.D., Lowry, A.R. & Miller, M.S., 2014. Static and dynamic support of western United States topography, *Earth planet. Sci. Lett.,* **402,** 234–246.

Biryol, C.B., Zandt, G., Beck, S.L., Özacar, A.A., Adiyaman, H.E. & Gans, R.C., 2010. Shear wave splitting along a nascent plate boundary: The North Anatolian Fault Zone, *Geophys. J. Int.,* **181,** 1201–1213.

Biryol, C.B., Beck, S.L., Zandt, G. & Özacar, A.A., 2011. Segmented African lithosphere beneath the Anatolian region inferred from teleseismic *P*-wave tomography, *Geophys. J. Int.,* **184,** 1037–1057.

Bonvalot, S. *et al.*, 2012. *World Gravity Map,* Commission for the Geological Map of the World, Eds. BGI-CGMW-CNES-IRD, Paris.

Boschi, L., Faccenna, C. & Becker, T.W., 2010. Mantle structure and dynamic topography in the Mediterranean Basin, *Geophys. Res. Lett.,* **37,** L20303, doi:10.1029/2010GL045001.

Chamorro, C.R., García-Cuesta, J.L., Mondéjar, M.E. & Pérez-Madrazo, A., 2014. Enhanced geothermal systems in Europe: an estimation and comparison of the technical and sustainable potentials, *Energy,* **65,** 250–263.

Chopelas, A. & Boehler, R., 1989. Thermal expansion measurement at very high pressure, systematic and a case for a chemical homogeneous mantle, *Geophys. Res. Lett.,* **16,** 1347–1350.

Çiner, A., Dogan, U., Yildirim, C., Akcar, N., Ivy-Ochs, S., Alfimov, V., Kubik, P.W. & Schluchter, C., 2015. Quaternary uplift rates of the Central Anatolian Plateau, Turkey: insights from cosmogenic isochron-burial nuclide dating of the Kizilirmak river terraces, *Quat. Sci. Rev.,* **107,** 81–97.

Cosentino, D., Schildgen, T.F., Cipollari, P., Faranda, C., Gliozzi, E., Hudáčková, N., Lucifora, S. & Strecker, M.R., 2011. Late Miocene surface uplift of the southern margin of the Central Anatolian Plateau, Central Taurides, Turkey, *Bull. geol. Soc. Am.,* **124**(1–2), 133–145.

Faccenna, C. & Becker, T.W., 2010. Shaping mobile belts by small-scale convection, *Nature,* **465**(7298), 602–605.

Faccenna, C., Bellier, O., Martinod, J., Piromallo, C. & Regard, V., 2006. Slab detachment beneath eastern Anatolia: a possible cause for the formation of the North Anatolian Fault, *Earth planet. Sci. Lett.,* **242,** 85–97.

Faccenna, C. *et al.*, 2014. Mantle dynamics in the Mediterranean, *Rev. Geophys.,* **52,** 283–332.

Fichtner, A., Trampert, J., Cupillard, P., Saygin, E., Taymaz, T., Capdeville, Y. & Villasenor, A., 2013a. Multiscale full waveform inversion, *Geophys. J. Int.,* **194**(1), 534–556.

Fichtner, A., Saygin, E., Taymaz, T., Cupillard, P., Capdeville, Y. & Trampert, J., 2013b. The deep structure of the North Anatolian Fault Zone, *Earth planet. Sci. Lett.,* **373,** 109–117.

Flament, N., Gurnis, M. & Müller, R.D., 2013. A review of observations and models of dynamic topography, *Lithosphere,* **5,** 189–210.

Forte, A.M., Moucha, R., Rowley, D.B., Quéré, S., Mitrovica, J.X., Simmons, N.A. & Grand, S.P., 2009. Recent tectonic plate decelerations driven by mantle convection, *Geophys. Res. Lett.,* **36**(23), L23301, doi: 10.1029/2009GL040224.

Fullsack, P., 1995. An arbitrary Lagrangian-Eulerian formulation for creeping flows and applications in tectonic models, *Geophys. J. Int.,* **120,** 1–23.

Gleason, G.C. & Tullis, J., 1995. A flow law for dislocation creep of quartz aggregates determined with the molten salt cell, *Tectonophys,* **247,** 1–23.

GLOBE Task Team *et al.* (eds), 1999. *The Global Land One-kilometer Base Elevation (GLOBE) Digital Elevation Model, Version 1.0,* National Oceanic and Atmospheric Administration, National Geophysical Data Center. Available at: http://www.ngdc.noaa.gov/mgg/topo/globe.html, last accessed 23 March 2014.

Göğüş, O.H., 2015. Rifting and subsidence following lithospheric removal in continental back-arcs, *Geology,* **43,** 3–6.

Göğüş, O. & Pysklywec, R.N., 2008a. Near surface diagnostics of dripping or delaminating lithosphere, *Geophys. Res. Lett.,* **113,** B11404, doi:10.1029/2007JB005123.

Göğüş, O.H. & Pysklywec, R.N., 2008b. Mantle lithosphere delamination driving plateau uplift and synconvergent extension in eastern Anatolia, *Geology,* **36**(9), 723–726.

Gök, R., Sandvol, E., Türkelli, N., Seber, D. & Barazangi, M., 2003. Sn attenuation in the Anatolian and Iranian plateau and surrounding regions, *Geophys. Res. Lett.,* **30**(24), doi:10.1029/2003GL018020.

Gray, R. & Pysklywec, R.N., 2012. Influence of sediment deposition on deep lithospheric tectonics, *Geophys. Res. Lett.,* **39,** L11312, doi:10.1029/2012GL051947.

Gvirtzman, A. & Nur, A., 2001. Residual topography, lithospheric structure and sunken slabs in the central Mediterranean. *Earth planet. Sci. Lett.,* **187,** 117–130.

Hartley, R., Watts, A.B. & Fairhead, J.D., 1996. Isostasy of Africa, *Earth planet. Sci. Lett.,* **137,** 1–18.

Hearn, T.M. & Ni, J.F., 1994. Pn velocities beneath continental collision zones: the Turkish-Iranian Plateau, *Geophys. J. Int.,* **117,** 273–283.

Heiskanen, W.A. & Meinesz, V.F.A., 1958. *The Earth and Its Gravity Field,* McGraw-Hill Book Company, INC, 470 pp.

Hirth, G. & Kohlstedt, D.L., 1996. Water in the oceanic upper mantle: implications for rheology, melt extraction and the evolution of the lithosphere, *Earth planet. Sci. Lett.,* **144,** 93–108.

Huvaz, Ö., 2009. Comparative petroleum systems analysis of the interior basins of Turkey: implications for petroleum potential, *Mar. Pet. Geol.,* **26,** 1656–1676.

Jolivet, L., Faccenna, C. & Piromallo, C., 2009. From mantle to crust: stretching the Mediterranean, *Earth planet. Sci. Lett.,* **285,** 198–209.

Karato, J., 1993. Importance of anelasticity in the interpretation of seismic tomography, *Geophys. Res. Lett.,* **20,** 1623–1626.

Kind, R. *et al.*, 2015. Thickness of the lithosphere beneath Turkey and surroundings from S-receiver functions, *Solid Earth Discuss.,* **7,** 1315–1346.

Kömeç-Mutlu, A. & Karabulut, H., 2011. Anisotropic Pn tomography of Turkey and adjacent regions, *Geophys. J. Int.,* **187**(3), 1743–1758.

Komut, T., Gray, R., Pysklywec, R.N. & Göğüş, O. H., 2012. Mantle flow uplift of western Anatolia and the Aegean: interpretations from geophysical analyses and geodynamic modeling, *J. geophys. Res.,* **117,** doi:10.1029/2012JB009306.

Kumar, N., Singh, A.P., Rao, M.R.K.P., Chandrasekhar, D.V. & Singh, B., 2009. Gravity signatures, derived crustal structure and tectonics of Achankovil Shear Zone, southern India, *Gondwana Res*., **16**(1), 45–55.

Kürkçüoğlu, B., Şen, E., Temel, A., Aydar, E. & Gourgaud, A., 2004. Interaction of asthenospheric and lithospheric mantle: the genesis of calc-alkaline volcanism at Mt. Erciyes Volcano, Central Anatolia, Turkey, *Int. Geol. Rev.,* **46**(3), 243–258.

Lachenbruch, A.H. & Morgan, P., 1990. Continental extension, magmatism and elevation: formal relations and rules of thumb, *Tectonophysics,* **174,** 39–62.

Laske, G., Masters, G., Ma, Z. & Pasyanos, M., 2013. Update on CRUST1.0 - A 1-degree Global Model of Earth's Crust, *Geophys. Res. Abstracts,* **15,** EGU2013-2658.

Molinari, I. & Morelli, A., 2011. EPcrust: a reference crustal model for the european plate, *Geophys. J. Int,* **185**(1), 352–364.

MTA, 2014. 'General Directorate Of Mineral Research And Exploration, Turkey'. Available at: http://www.mta.gov.tr, last accessed 17 April 2014.

Özelçi, H.F., 1973. Gravity anomalies of the Eastern Mediterranean, *Bull. Miner. Res. Explor.,* **80,** 54–92.

Özeren, M.S. & Holt, W.E., 2010. The dynamics of the eastern Mediterranean and eastern Turkey, *Geophys. J. Int.,* **183,** 1165–1184.

Özsayin, E. *et al.*, 2013. Plio-Quaternary extensional tectonics of the Central Anatolian Plateau: a case study from the Tuz Gölü Basin, Turkey, *Turk. J. Earth Sci.,* **22,** 691–714.

Paul, A., Karabulut, H., Kömeç-Mutlu, A. & Salaün, G., 2014. A comprehensive and densely sampled map of shear-wave azimuthal anisotropy inthe Aegean–Anatolia region, *Earth planet. Sci. Lett.,* **389,** 14–22.

Pekeris, C.L., 1935. Thermal convection in the interior of the Earth, *Geophys. J. Int.,* **3,** 343–367.

Piromallo, C. & Morelli, A., 2003. *P* wave tomography of the mantle under the Alpine–Mediterranean area, *J. geophys. Res.,* **108,** doi:10.1029/2002JB001757.

Pysklywec, R.N., 2006. Surface erosion control on the evolution of the deep lithosphere, *Geology,* **34**(4), 225–228.

Pysklywec, R.N. & Beaumont, C., 2004. Interpolate tectonics: feedback between radioactive thermal weakening and crustal deformation driven by mantle lithosphere instabilities, *Earth planet. Sci. Lett.,* **221,** 275–292.

Pysklywec, R.N., Beaumont, C. & Fullsack, P., 2002. Lithospheric deformation during the early stages of continental collision: numerical experiments and comparison with South Island, New Zealand, *J. geophys. Res.,* **107**(B7), 2133, doi:10.1029/2001JB000252.

Reilinger, R. *et al.*, 2006. GPS constraints on continental deformation in the Africa-Arabia-Eurasia continental collision zone and implications for the dynamics of plate interactions, *J. geophys. Res.,* **111,** doi:10.1029/2005JB004051.

Salaün, G. *et al.*, 2012. High-resolution surface wave tomography beneath the Aegean–Anatolia region: constraints on upper-mantle structure, *Geophys. J. Int.,* **190,** 406–420.

Sandvol, E., Turkelli, N., Zor, E., Gok, R., Bekler, T., Gurbuz, C., Seber, D. & Barazangi, M., 2003. Shear wave splitting in a young continent-continent collision: an example from Eastern Turkey, *Geophys. Res. Lett.,* **30**(24), 8041, doi:10.1029/2003GL017390.

Schildgen, T.F., Cosentino, D., Bookhagen, B., Niedermann, S., Yildirim, C., Echtler, H., Wittmann, H. & Strecker, M.R., 2012. Multi-phased uplift of the southern margin of the Central Anatolian plateau, Turkey: a record of tectonic and upper mantle processes, *Earth planet. Sci. Lett.,* **317–318,** 85–95.

Shaw, M. & Pysklywec, R.N., 2007. Anomalous uplift of the Apennines and subsidence of the Adriatic: the result of active mantle flow? *J. geophys. Res.,* **34,** L04311, doi:10.1029/2006GL028337.

Simons, F.J., Zuber, M.T. & Korenaga, J., 2000. Isostatic response of the Australian lithosphere: estimation of effective elastic thickness and anisotropy using multitaper spectral analysis, *J. geophys. Res.,* **105,** 19 163–19 184.

Şimşek, Ş., 2001. An overview of geothermal developments in Turkey, in *ITIT International Symposium Extended Abstracts,* Japan, pp. 17–23.

Tankut, A., Wilson, M. & Yihunie, T., 1998. Geochemistry and tectonic setting of Tertiary volcanism in the Güvem area, Anatolia, Turkey, *J. Volcanol. Geotherm. Res.,* **85,** 285–301.

Tezcan, A.K., 1995. Geothermal explorations and heat flow in Turkey, in *Terrestrial Heat Flow and Geothermal Energy in Asia*, pp. 23–42, eds Gupta, M.L. & Yamano, M., Oxford and IBH.

Tezcan, A.K. & Turgay, M.I., 1991. Catalogue of heat flow density data: Turkey, in *Geothermal atlas of Europe, International Association for Seismology and Physics of the Earth's Interior, International Heat Flow Commission; Central Institute for Physics of the Earth*, pp. 84–85, eds Hurtig, E. *et al.*, Hermann Hack Verlagsgesellschaft.

Tezel, T., Shibutani, T. & Kaypak, B., 2013. Crustal thickness of Turkey determined by receiver function, *J. Asian Earth Sci.,* **75,** 36–45.

Vanacore, E.A., Taymaz, T. & Saygin, E., 2013. Moho structure of the Anatolian Plate from receiver function analysis, *Geophys. J. Int.,* **193**(1), 329–337.

Vinnik, L., Erduran, M., Oreshin, S., Kosarev, G., Kutlu, Y.A., Çakir, Ö. & Kiselev, S., 2014. Joint inversion of *P* and *S* receiver functions and dispersion curves of Rayleigh waves: the results for the Central Anatolian Plateau, *Izv. Phys. Solid Earth,* **50**(5), 622–631.

Yildirim, C., Schildgen, T.F., Echtler, H., Melnick, D. & Strecker, M.R., 2011. Late Neogene and active orogenic uplift in the Central Pontides associated with the North Anatolian Fault: implications for the northern margin of the Central Anatolian Plateau, Turkey, *Tectonics,* **30**(5), doi:10.1029/2010TC002756.

Yildirim, C., Melnick, D., Ballato, P., Schildgen, T.F, Echtler, H., Erginal, A.E., Kiyak, N.G. & Strecker, M.R., 2013. Differential uplift along the northern margin of the Central Anatolian Plateau: inferences from marine terraces, *Quat. Sci. Rev.,* **81,** 12–28.

Yolsal-Çevikbilen, S., 2014. Seismic anisotropy along the Cyprean arc and northeast Mediterranean Sea inferred from shear wave splitting analysis, *Phys. Earth planet. Inter.,* **233,** 112–134.

Yürür, M.T., Temel, A. & Köse, O., 2002. Evidences of Extensional Tectonics at the Southern Boundary of the Galatean Volcanic Province, NW Central Anatolia, *Geol. Bull. Turkey,* **45**(1), 85–98.